Available online at www.sciencedirect.com
ScienceDirect
Acta Materialia 54 (2006) 5607–5615
Acta MATERIALIA
www.actamat-journals.com

# Measurement and modelling of the nanoindentation response of shape memory alloys

A.J. Muir Wood, T.W. Clyne *

*Department of Materials Science and Metallurgy, Cambridge University, Pembroke Street, Cambridge CB2 3QZ, UK*

Received 25 April 2006; received in revised form 18 July 2006; accepted 8 August 2006
Available online 23 October 2006

**Abstract**

A nickel–titanium shape memory alloy was subjected to nanoindentation over a range of temperature (up to 200 °C), such that the starting material was either predominantly martensitic or largely composed of the parent phase. The load–displacement data were interpreted to give information about whether the imposed strain was being at least partly accommodated by the martensitic phase transformation, i.e. whether superelastic deformation was taking place. This interpretation was assisted by finite element simulation of the evolving strain field under an indenter, with or without the superelastic deformation mechanism being operative. It is concluded that the nanoindentation response can be used to determine whether the material is capable of exhibiting superelastic deformation, provided appropriate procedures are employed. Spherical indenters are more suitable than sharp tips. A relatively low value for the remnant indent depth ratio (depth after unloading/depth at peak load) is indicative that superelasticity is occurring. The procedure was found to be viable with a small radius (10 μm) spherical indenter, so it can be employed to explore local variations in superelastic response.


*Keywords:* Nickel–titanium; Shape memory; Nanoindentation; Finite element modelling

## 1. Introduction

Shape memory alloys (SMAs) have been intensively studied over the past 20 years. They can take many forms, but the most commonly studied SMA system is nickel–titanium, usually with a composition close to Ni–50 at.%Ti [1–7]. Below some temperature, $M_f$, defined as that at which martensitic transformation of the parent phase to the martensitic phase is complete, the martensitic phase (a monoclinic B19′ structure in the Ni–Ti case) is thermodynamically stable. On heating to a higher temperature $A_f$, reversion to the parent phase (a cubic B2 structure in the Ni–Ti case) is complete. Above $A_f$, SMAs can demonstrate superelasticity (SE), in which relatively large mechanically imposed strains (up to $\sim 8\%$) can be accommodated by transformation of the parent phase to metastable martensitic variants. These variants revert to the parent phase on removal of the applied load. The shape memory effect (SME) can also be observed in these alloys. Application of stress to a specimen at a temperature below $M_f$ can lead to the strain being accommodated by reorientation of martensitic variants. On heating above $A_f$, however, the martensite can transform to the parent phase in such a way that the original shape is recovered. Subsequent (unloaded) cooling below $M_f$ can occur without further shape change. Repeated cycles of deformation, heating to give shape recovery, are possible and other types of shape memory behaviour can also be observed.

There is growing interest in applying nanoindentation to SMAs, partly because this technique can be used to investigate small volumes of material and thus can be used to study local variations in mechanical response. If nanoindentation could reliably be used to determine the local SE and SME characteristics then it would be particularly useful for the study of joints and other regions of compositional and microstructural variation in SMA structures. There are, however, various complications associated with

* Corresponding author.
*E-mail address:* twc10@cam.ac.uk (T.W. Clyne).

1359-6454/$30.00 
doi:10.1016/j.actamat.2006.08.013

the imposition of complex strain fields on SMAs, particularly if they are applied over a range of temperatures. Interpretation of their nanoindentation response thus requires considerable care.

Most previous superelasticity-oriented nanoindentation studies on SMAs have either involved loads insufficient to cause permanent deformation [8–10] or have compared the behaviour of superelastic SMAs with that of entirely different material, having no shape memory properties [11,12]. A more systematic approach, facilitated by the increasing availability of indentation hot stages, involves comparing the responses of a SMA above and below $A_f$, i.e. in regimes where a SE response would and would not be expected. There have been several comprehensive nanoindentation studies of the SME [13–19], but lack of hot stages has inhibited their extension to encompass SE.

While various authors [4,5,20–24] have demonstrated that there is a difference in hardness and Young's modulus between SMAs in their two states, it is acknowledged that this difference is hard to characterize. After indentation with a Berkovich tip, it is easy to obtain hardness and Young's modulus values from the indentation plot, for example using the Oliver and Pharr technique [25], but these data are of little use if no reliable distinction between the two states is possible. Another parameter that is easily acquired from indentation data is the remnant depth ratio, defined as the ratio of the final (unloaded), or remnant, depth, $d_{rem}$, to the peak depth, $d_{peak}$.

It is in any event clear that several important issues in this field remain unresolved. In the present paper, an attempt is made to analyse the main features of nanoindentation data obtained from SMAs and hence to identify optimal procedures for using the technique to measure SMA characteristics on a local scale.

## 2. Experimental procedures

Raw material was supplied by Memory Metalle GmbH in the form of a rod of diameter 15.25 mm and composition Ti–50.2 at.%Ni. In the as-received state, the rod was fully martensitic. This alloy can undergo parent-to-martensite phase transformations under imposed mechanical strain, with a volume change of 0.34% and a shear strain of 13%. The transformation can also be induced in that direction by cooling or, in the reverse direction, by heating. Transformation temperatures (in the absence of imposed stress or strain) were determined by differential scanning calorimetry (DSC), using a Q1000 Thermal Analysis instrument. X-ray diffraction (XRD) scans were performed over a range of temperature, using a Siemens D500 X-ray diffractometer with Cu K$\alpha$ ($\lambda = 0.154056$ nm) radiation.

Indentation work was carried out using a MicroMaterials Nanotest 600 Nanoindenter. High load experiments ($P \gtrsim 400$ mN) were performed using the MicroTest pendulum, while low load experiments were carried out with the NanoTest pendulum. Indentation was undertaken using a Berkovich tip and also two spherical indenters ($r = 650$ and 10 μm). Both the Berkovich and the smaller spherical tip were fitted with tip-heaters, which were used in conjunction with a sample heating stage to give improved thermal stability during high temperature indentation. Experiments were conducted at up to 200 °C.

## 3. Finite element modelling

A model of the indentation process was developed using ABAQUS, building on previous work in this area [26–30]. In order to simulate superelastic behaviour, a Nitinol user subroutine (UMAT), supplied by ABAQUS, was employed [31]. The UMAT employs a rationale proposed by Auricchio and Taylor [32,33], which is based on the concept of generalized plasticity. The work-hardening behaviour is assumed to exhibit a large degree of tensile-compressive symmetry [34]. This is a potential source of error, since there is evidence [35–37] that these alloys can be significantly asymmetric in their yielding and work-hardening behaviour. A comprehensive treatment would require knowledge of the complete yield envelope and the work-hardening characteristics as a function of stress state. Neither this information nor a sub-routine for its implementation are currently available.

In any event, the subroutine employed requires the stress–strain relationship of the system. This was assumed to conform to the shape shown in Fig. 1 and the parameters shown on this plot were used as input data for the model. The large degree of tensile–compressive symmetry is apparent. A comparison is shown in Fig. 2 between experimental stress–strain data obtained during uniform tensile and compressive loading of the Ni–Ti rod and best-fit modelled curves obtained by selection of the parameters shown in Fig. 1. It is clear that, while the behaviour under tensile

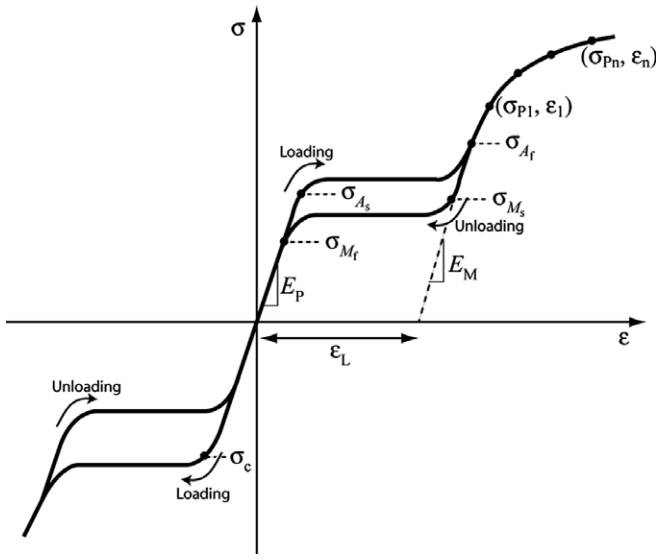


Fig. 1. Stress–strain relationship for a material exhibiting superelastic deformation, showing the input parameters for the ABAQUS model.

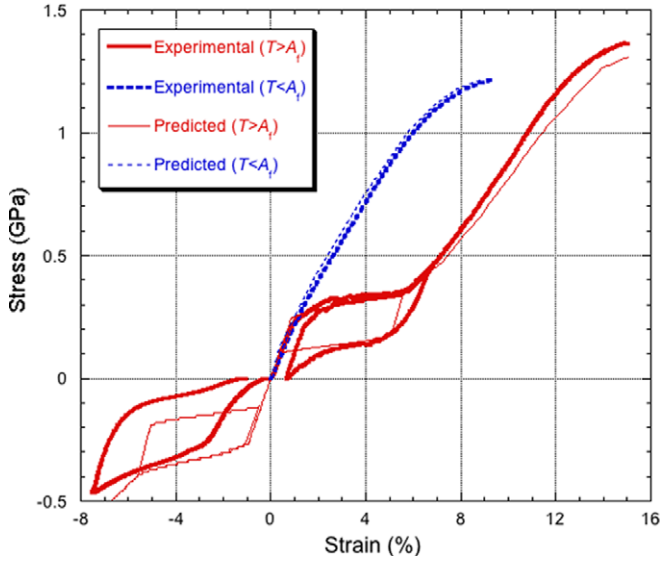


Fig. 2. Comparison between experimental stress–strain data obtained during uniaxial loading in tension and compression of the Ni–Ti alloy being studied and corresponding curves obtained from ABAQUS modelling, using best fit values for the parameters shown in Fig. 1.

loading is quite accurately represented, the constraints on the input data parameterization are such that the compressive behaviour is less reliably captured.

## 4. Results and discussion

### 4.1. Phase transformation hysteresis behaviour

Differential scanning calorimetry traces (Fig. 3) confirmed that the material transforms to the superelastic parent phase on heating above about 100 °C. On cooling, the material only reverts fully to the martensitic phase when the temperature is reduced to slightly below ambient. In order to examine material behaviour through the full range of states, prior cooling in liquid nitrogen was therefore undertaken, to ensure that the initial state was fully martensitic. The X-ray diffraction data shown in Fig. 4 highlight the hysteresis effects. While Fig. 4a demonstrates that, on heating, the parent phase does not start to form until about 75 °C, and only becomes complete at 100 °C, Fig. 4b shows that, on cooling, martensite only starts to form at about 50 °C and some parent phase persists down to room temperature.

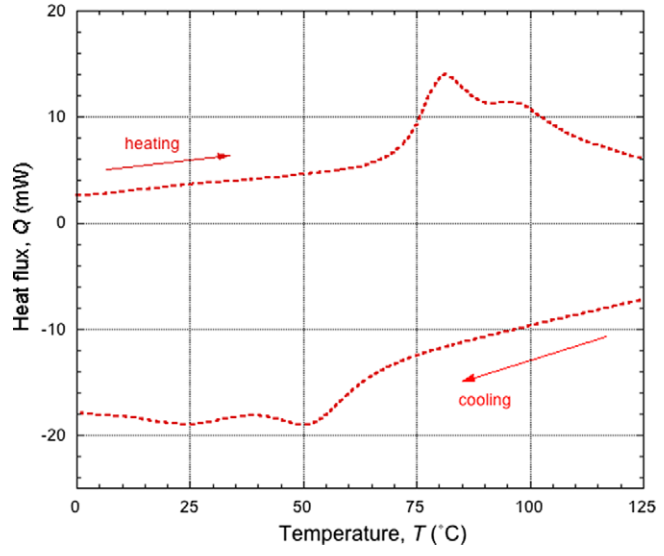


Fig. 3. DSC plots for the Ni–Ti alloy being studied, during heating and cooling. It can be inferred from these curves that the values of $A_s$ and $M_s$ are about 70 and 60 °C, respectively.

### 4.2. Indentation

Indentation measurements with a Berkovich (sharp) tip yielded the plots shown in Fig. 5a. While these might appear to reveal qualitatively different behaviour for the two crystallographic states, once the difference in their mechanical properties is taken into account there is no real

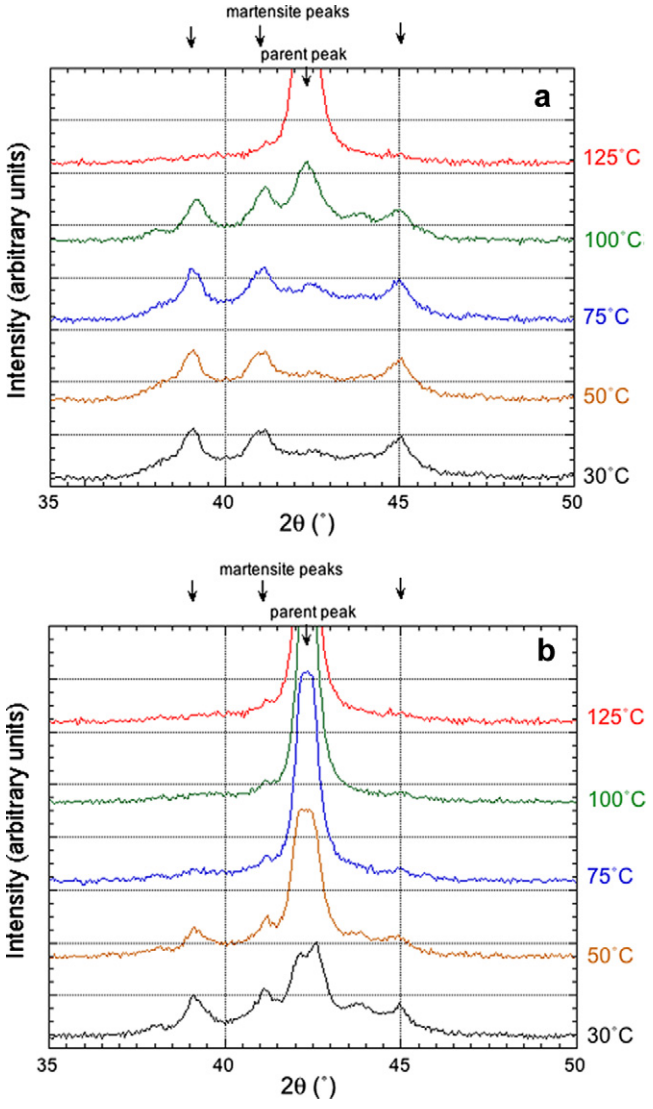


Fig. 4. XRD spectra obtained during: (a) heating and (b) cooling.

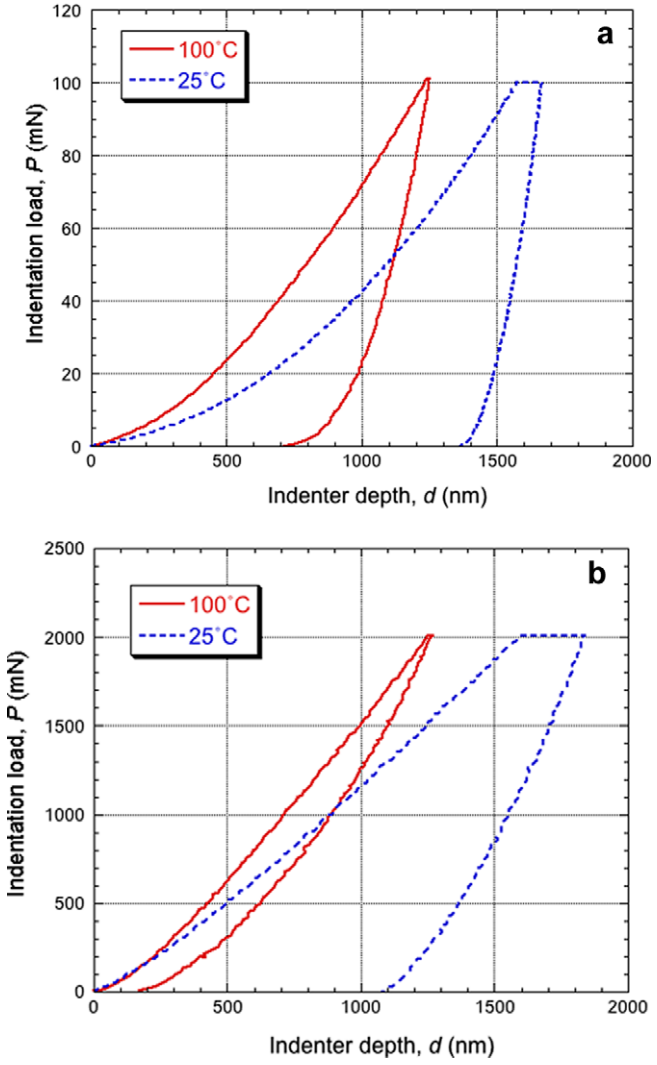


Fig. 5. Load–displacement plots obtained during indentation carried out at temperatures such that the starting material would primarily be either in the parent phase (100 °C) or in the martensitic state (25 °C), using (a) Berkovich and (b) large spherical ($r = 650$ μm) indenter tips. The dwell period at maximum load was 120 s.

evidence in these plots of superelastic recovery. When a spherical tip is used, however, the distinction between the two plots becomes much clearer (see Fig. 5b). In this case, there is evidence of superelastic recovery when the material is initially in the parent phase state, whereas there is little or no such recovery at lower temperatures, when the starting material is martensitic.

This difference can be explained in terms of the peak strain levels beneath the two types of tip. Under a Berkovich tip, high peak strain levels tend to be generated immediately below the tip, even at low applied loads. Superelastic deformation, which can only accommodate strains of up to ~ 8%, is not expected to be the sole, or even the predominant, deformation mode in such high strain regions, so the observation that most of this strain is not recovered on unloading is unsurprising. Since superelasticity cannot fully accommodate the deformation, this high strain will result in the generation of a high density of dislocations, through conventional plastic deformation. The presence of an increased density of dislocations will limit the formation of martensite within the parent phase, since they stabilize the parent phase and will oppose its transformation to martensite. Any martensite that does form, however, may do so irreversibly, since the high dislocation density will both pin and aid the stabilization of martensitic variants, limiting their reversion to the parent phase, on the removal of the applied load. Thus the high peak strains under a sharp indenting tip will severely inhibit any superelastic recovery.

Beneath a spherical tip, on the other hand, peak strain levels are much lower, although, since they increase with increasing load (i.e. the loading is not self-similar), they might approach those under a Berkovich tip at high applied loads. The observation that much of the strain is recovered on unloading with the spherical tip, for temperatures around or above $A_f$ (~100 °C), is therefore consistent with this, and the technique appears to show promise as a method of testing whether or not the material can exhibit superelastic deformation and recovery. Since the strain is much lower, not only will the material be able to accommodate this largely through superelastic phase transformations, but there will be little or no generation of dislocations, so superelastic recovery will not be inhibited.

Indenting with a large spherical tip is rather unwieldy, especially if the technique is to be used to study thin films or the effects of local microstructural variations. It is obviously of interest, therefore, to explore indentation with a small spherical tip. The load–displacement plots shown in Fig. 6 were obtained using a diamond cone polished to a tip radius of about 10 μm. At first glance, these plots appear similar to those obtained with the Berkovich tip

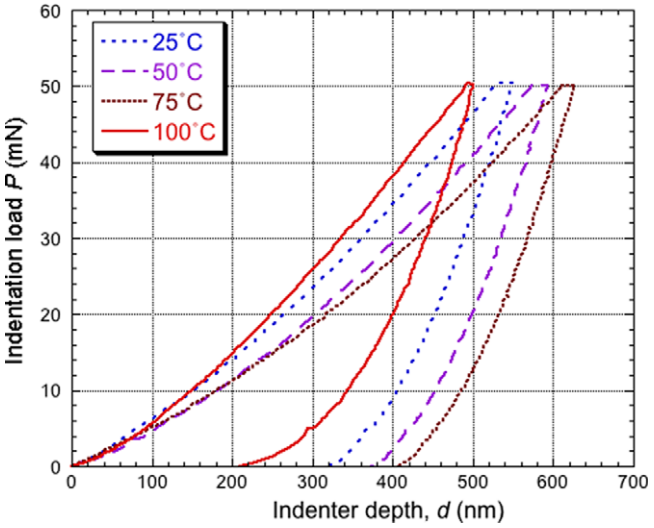


Fig. 6. Load–displacement plots obtained during indentation carried out at various temperatures around and below $A_f$, using a small spherical ($r = 10$ μm) indenter. The dwell period at maximum load was 10 s.

(Fig. 5(a)), but closer examination shows that they are in fact displaying evidence of the transition from the martensitic to the parent phase, and that superelastic recovery is taking place. The differences between the traces at 25 and 100 °C are relatively small, but there is clearly more strain recovery during the final stages of unloading at the higher temperature. This is illustrated by the plot in Fig. 7a, which shows the remnant depth ratio (unloaded depth/peak depth), as a function of applied load, for testing at these two temperatures. The smaller tip used in this case will have generated higher strains, since the strain increases with decreasing radius. The strain levels will not, however, have approached those typically present under a Berkovich (sharp) tip.

It is the intermediate temperature (50 and 75 °C) plots in Fig. 6, however, which provide the clearest evidence of the transition between superelastic and non-superelastic behaviour, since they exhibit much less recovery than is observed around $A_f$ (~100 °C). As the test temperature is raised, the maximum depth of indentation is in general expected to increase, due to conventional softening. The contrast with superelastic behaviour is thus expected to be higher at higher temperatures, and this is clearly

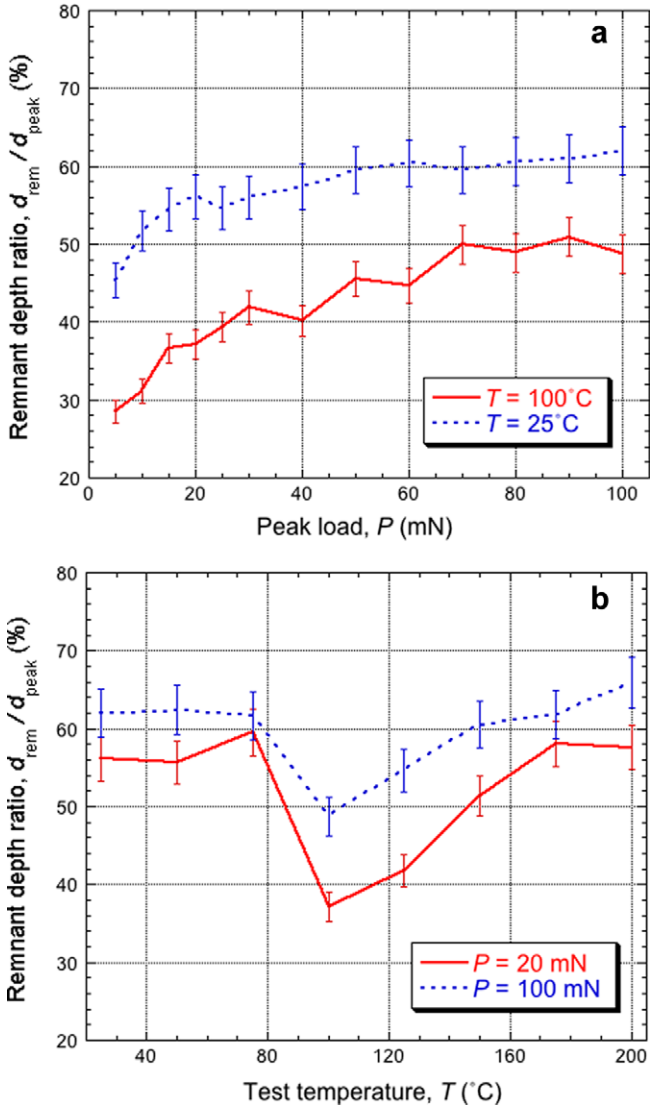


Fig. 7. Plots of remnant depth ratio as a function of: (a) peak load, at two different test temperatures and (b) test temperature, for two different loads. Testing was carried out using a small spherical ($r = 10$ μm) indenter, with a dwell period at maximum load of 10 s.

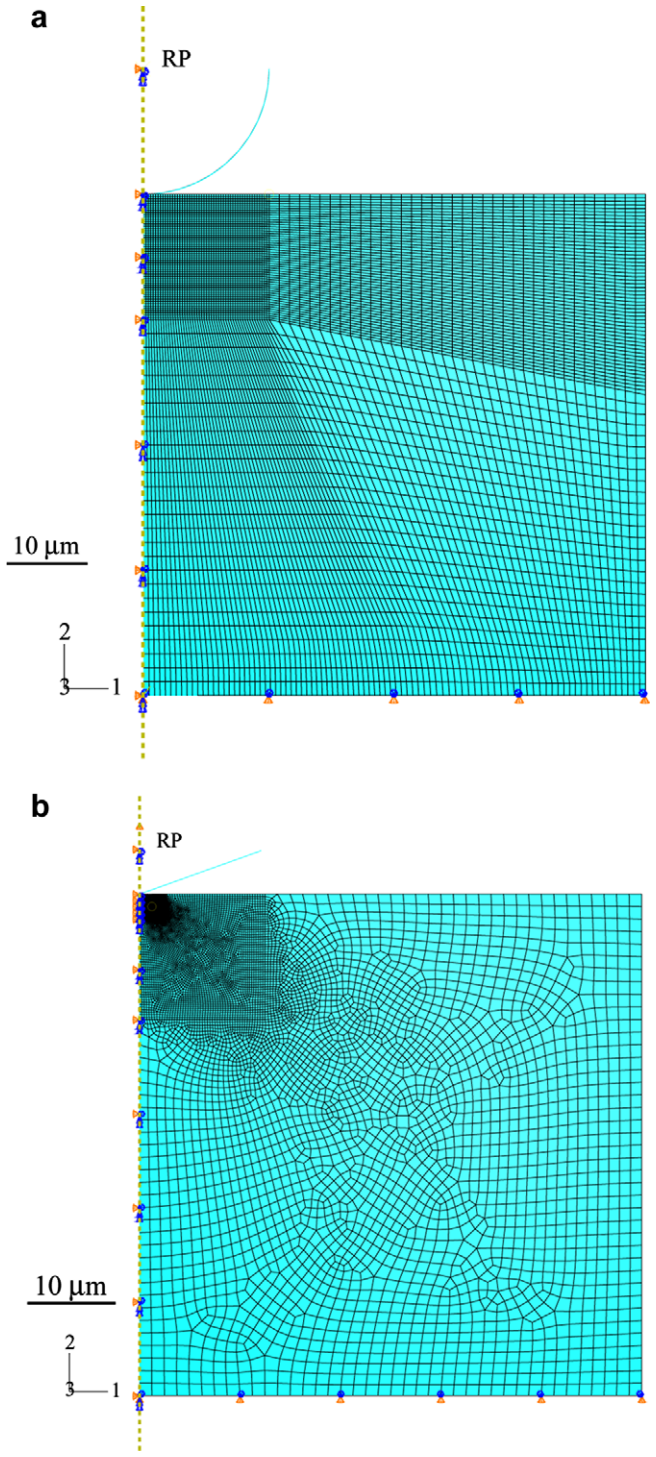


Fig. 8. FEM (axi-symmetric) meshes used for simulation of indentation with (a) spherical ($r = 10$ μm) and (b) conical (cone angle = 70°) tips.

observed. As the temperature is increased above $A_f$ not only does the maximum depth of indentation drop, but the remnant depth ratio also drops noticeably (Fig. 7b), indicating that a strain recovery mechanism is operating on unloading around $A_f$, which was not operative at lower temperatures. It can be seen that this difference in remnant depth ratio persists over a range of applied load, although the change on moving into the superelastic regime is somewhat greater for lower loads. This is clearly consistent with the concept that higher loads may lead to peak strains beyond the superelastic limit, generating dislocations and reducing the likelihood of full reversion from martensite to parent phase on removal of the applied load. In any event, it appears clear that the technique, and the use of the remnant depth ratio as a detection parameter, are suitable for local testing of whether or not a material can exhibit superelastic deformation.

It is also worth noting that the observed behaviour at higher temperatures (100–200 °C in Fig. 7b) is consistent with these interpretations. It is well known [38] that superelasticity can only occur when the stress required to induce martensite is below that required for conventional plastic deformation (dislocation glide) in the parent phase. Since this becomes easier at high temperatures, as a consequence of dislocation motion being thermally activated, and since martensitic nucleation becomes harder, following a Clausius–Clapeyron dependence, it is expected that, at some temperature above $A_f$, superelastic deformation will become impossible. This explains the observed increase in remnant depth ratio, to levels comparable to those observed below $A_f$, when the temperature is raised to ~160 °C. At this temperature, conventional plastic deformation is easier than superelastic deformation and hence dominates the behaviour.

### 4.3. Finite element modelling

The meshes used for the finite element modelling (FEM) are shown in Fig. 8. These are similar to those used in previous work [26–30], with a fine mesh close to the indenter and a coarser mesh further away. Previous work [26] has demonstrated that a conical tip represents a good approximation to a Berkovich tip, if the cone angle is set to 70°. The cone was given a tip radius of 150 nm, comparable to values typically quoted by tip suppliers. As a result of the extremely high strains present beneath an indenting cone, it was necessary to remesh after each step and, since the Nitinol UMAT subroutine could not be used in conjunction with this remeshing, only indentation of the martensitic phase could be simulated with a conical indenter. With the spherical indenter, on the other hand, indentation of both the martensitic phase and the parent phase could be simulated.

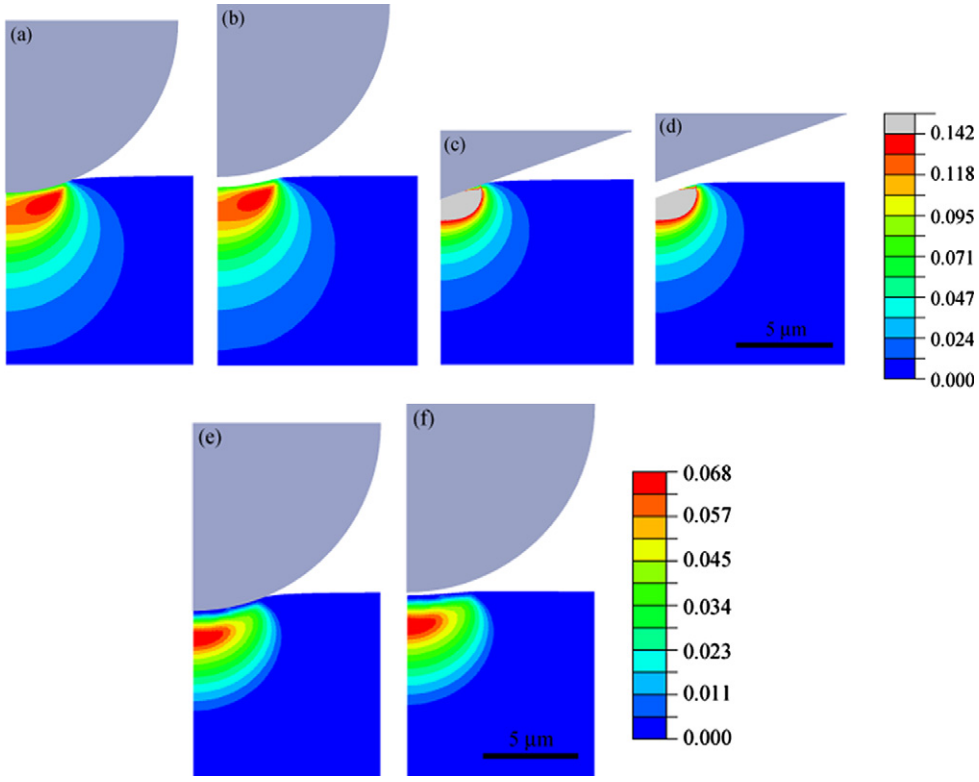


Fig. 9. Predicted distributions of equivalent plastic strain during and after indentation of martensitic Ni–Ti ((a)–(d)) and parent phase Ni–Ti ((e) and (f)). Strain fields are for (a) a load of 100 mN and (b) after load removal for an indenting sphere ($r = 10$ μm), and for (c) a load of 100 mN and (d) after load removal for an indenting cone (angle = 70°). Also shown, for the spherical indenter, are strain fields for the parent phase (e) under 75 mN load and (f) after load removal.

Predicted strain fields are shown in Fig. 9. It can be seen, on comparing Fig. 9a and b with Fig. 9c and d, that the peak strain levels are much higher with the conical indenter, although the strain field remote from the vicinity of the tip is similar in the two cases. There is also much less recovery on unloading with the conical indenter. When superelasticity is introduced (Fig. 9e and f), the peak plastic strain is much lower. The phase transformation (superelastic) strain has clearly accommodated a considerable part of the total strain and, on unloading, strain recovery is predicted to be substantial, in agreement with experimental observations.

However, on comparing load–displacement plots obtained experimentally with those from the FEM simulations, some discrepancies become apparent. This can be seen in Fig. 10. Good agreement is observed for both spherical and sharp (conical) indenter shapes, when there is no superelastic deformation (i.e. when indenting the martensitic phase). The agreement is less convincing, however, when superelastic deformation occurs (i.e. when indenting the parent phase). The predicted peak indentation depth is significantly greater than that measured experimentally and the predicted extent of recovery (remnant depth ratio) is also appreciably larger than that observed. This suggests that other modes of deformation, presumably conventional plastic flow, are exerting a significant effect on the observed experimental behaviour. This also ties in with the discussion above about the limited capability of the UMAT subroutine to accommodate compressive work-hardening characteristics differing substantially from those observed under tensile loading.

In any event, it seems clear that simulation of the changing strain field during the process is not fully capturing the associated mechanical characteristics. This is unsurprising, since the interactions between plastic (dislocation glide) and superelastic (phase transformation) strains will in reality be highly complex during indentation, which involves high strain gradients and substantial triaxial constraint. As discussed above, even at low strains, some nucleation and glide of dislocations is expected. The density and distribution of dislocations will affect the capacity for nucleation and growth of martensitic variants in the parent phase, and for their subsequent reversion. Further development of the simulation algorithms for combined superelastic/plastic straining, and validation with simpler loading geometries, are required before they can reliably be applied to the indentation process. The FEM predictions presented here nevertheless clearly indicate that the peak strain levels under a sharp tip are much higher than those under a sphere. They have also confirmed that a small spherical indenter can be used to test for superelastic material response, by ensuring that the straining is at least predominantly superelastic (provided the material is capable of deforming in this mode), and that experimental data can reveal that this is occurring.

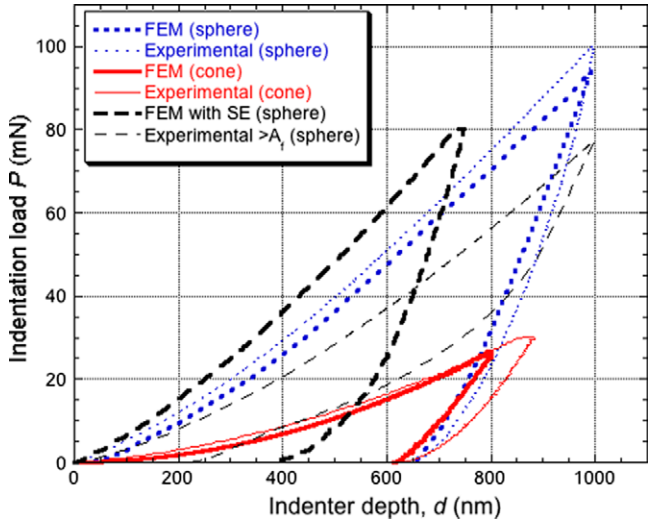


Fig. 10. Comparison between predicted (FEM) and measured load–displacement plots during loading and unloading, with spherical and sharp (conical) indenters and, for the case of the spherical indenter, with and without the superelastic (martensitic phase transformation) deformation mechanism being operative.

## 5. Conclusions

The following conclusions can be drawn from this work.

1. A nickel–titanium alloy has been studied, which transforms from fully martensitic at low (room) temperatures to fully parent at high temperatures ( $\gtrsim 100$ °C). The parent–martensite transformation has an associated volume change of 0.34% and can be induced by mechanical straining. The alloy was subjected to nanoindentation over a range of temperatures (up to 200 °C). The load–displacement data have been interpreted to give information about whether the imposed strain was being accommodated at least partly by the martensitic phase transformation, i.e. whether superelastic deformation was taking place. This interpretation was assisted by finite element simulation of the evolving strain field under an indenter, with and without the superelastic deformation mechanism being operative.
2. Using a Berkovich (sharp) tip, little difference was observed between load–displacement plots obtained under conditions such that superelastic deformation was or was not expected to be possible. This is attributed to the response of the material being dominated by regions of high strain immediately beneath the indenter tip, well beyond the levels that can be accommodated by superelasticity. The presence of such high strains was confirmed by finite element modelling, although (as a result of frequent remeshing being needed during simulation runs with a sharp indenter tip) they could only be carried out for indentation of the martensitic phase (no superelasticity possible). The high strain beneath the indenting tip promotes conventional plastic deformation and the resulting

increase in dislocation density is expected to both limit the formation of martensite and inhibit its subsequent reversion to the parent phase.

3. By using a spherical indenter, however, beneath which peak strain levels are much lower, operation of the superelastic deformation mechanism can reliably be detected. Differences between observed load–displacement plots, with and without superelastic deformation, were most pronounced with a large radius indenter. Use of a large diameter indenter makes it difficult to study thin films or the effects of local microstructural variations, but the procedure is viable even with a small (10 μm radius) spherical indenter. It has been shown that the dependence of the remnant indent depth ratio (unloaded/at peak load) on test temperature can be used as an indicator of whether superelasticity is occurring. A sharp drop in this ratio tends to be observed at around $A_f$, when the superelastic recovery mechanism can no longer operate. Finite element simulations were consistent with experimental observations of such differences in recovery after indentation with a small spherical indenter, with and without superelastic deformation taking place, although there were some discrepancies with regard to the details of the load–displacement plots for the superelastic case. Further refinement of the modelling algorithms, simulating interactions between superelastic and non-superelastic deformation modes, are required for fully reliable predictions. These should fully incorporate any tensile–compressive asymmetry exhibited by the material – in fact, ideally, they should take account of the complete stress state dependence of yielding and work-hardening characteristics.

## Acknowledgement

Funding has been provided by EPSRC, through a studentship and a Platform Grant.

## References

[1] Saburi T. Ti–Ni shape memory alloys. In: Otsuka K, Wayman CM, editors. Shape memory materials. Cambridge: CUP; 1998. p. 49–96.
[2] Van Humbeeck J, Stalmans R, Besselink PA. Shape memory alloys. In: Helsen JA, Breme HJ, editors. Metals as biomaterials. Wiley; 1998. p. 73–100.
[3] Van Humbeeck J, Stalmans R. Shape memory alloys types and functionalities. In: Schwartz M, editor. Encyclopaedia of smart materials. Wiley; 2002. p. 951–64.
[4] Van Humbeeck J, Stalmans R. Characteristics of shape memory alloys. In: Otsuka K, Wayman CM, editors. Shape memory materials. Cambridge: CUP; 1998. p. 149–83.
[5] Van Humbeeck J, Chandrasekaran M, Delaey L. Shape memory alloys: materials in action. Endeavour 1991;15:148–54.
[6] Van Humbeeck J. Shape memory alloys: a material and a technology. Adv Eng Mater 2001;3:837–50.
[7] Van Humbeeck J. The martensitic transformation. In: Shaller R, Fantozzi G, Gremaud G, editors. Mechanical spectroscopy. Trans Tech Publications; 2001. p. 382–415.
[8] Ma X-G, Komvopoulos K. Pseudoelasticity of shape-memory titanium-nickel films subjected to dynamic nanoindentation. Appl Phys Lett 2004;84:4274–6.
[9] Ma X-G, Komvopoulos K. Nanoscale pseudoelastic behavior of indented titanium–nickel films. Appl Phys Lett 2003;83:3773–5.
[10] Ma X-G, Komvopoulos K. In situ transmission electron microscopy and nanoindentation studies of phase transformation and pseudoelasticity of shape-memory titanium–nickel films. J Mater Res 2005;20:1808–13.
[11] Ni W, Cheng Y-T, Grummon DS. Microscopic superelastic behavior of a nickel–titanium alloy under complex loading conditions. Appl Phys Lett 2003;82:2811–3.
[12] Ni W, Cheng Y-T, Grummon DS. Microscopic shape memory and superelastic effects under complex loading conditions. Surf Coat Techn 2004;177–178:512–7.
[13] Gall K, Kreiner P, Turner D, Hulse M. Shape-memory polymers for microelectromechanical systems. J Microelectromech Syst 2004; 13:472–83.
[14] Ni W, Cheng Y-T, Grummon DS. Shape recovery and stress-induced martensite in TiNi following indentation and wear loading. J Phys IV 2003;112:1147–50.
[15] Ni W, Cheng Y-T, Grummon DS. Recovery of microindents in a nickel–titanium shape-memory alloy: a self-healing effect. Appl Phys Lett 2002;80:3310–2.
[16] Shaw GA, Trethewey JS, Johnson AD, Drugan WJ, Crone WC. Thermomechanical high-density data storage in a metallic material via the shape-memory effect. Adv Mater 2005;17:1123–7.
[17] Shaw GA, Stone DS, Johnson AD, Ellis AB, Crone WC. Shape memory effect in nanoindentation of nickel–titanium thin films. Appl Phys Lett 2003;83:257–9.
[18] Liu C, Zhao Y, Sun Q, Yu T, Cao Z. Characteristic of microscopic shape memory effect in a CuAlNi alloy by nanoindentation. J Mater Sci 2005;40:1501–4.
[19] Liu C, Zhao Y-P, Yu T. Measurement of microscopic deformation in a CuAlNi single crystal alloy by nanoindentation with a heating stage. Mater Design 2005;26:465–8.
[20] Van Humbeeck J, Delaey L. A comparative review of the (Potential) shape memory alloys. In: Hornbogen E, Jost N, editors. The martensitic transformation in science and technology. DGM Informationsgesellschaft; 1989. p. 5–25.
[21] Torra V. The science and technology of shape memory alloys. Barcelona: Impresrapit; 1987.
[22] Pelletier H, Muller D, Mille P, Grob JJ. Structural and mechanical characterisation of boron and nitrogen implanted NiTi shape memory alloy. Surf Coat Techn 2002;158–159:309–17.
[23] Frick CP, Ortega AM, Tyber J, Maksound AEM, Maier HJ, Liu Y, et al. Thermal processing of polycrystalline NiTi shape memory alloys. Mater Sci Eng A: Struct 2005;405:34–49.
[24] Qian L, Li M, Zhou Z, Yang H, Shi X. Comparison of nanoindentation hardness to microhardness. Surf Coat Techn 2005;195:264–71.
[25] Oliver WC, Pharr GM. An improved technique for determining hardness and elastic modulus using load and displacement sensing indentation experiments. J Mater Res 1992;7:1564–83.
[26] Dao M, Chollacoop N, Van Vliet KJ, Venkatesh TA, Suresh S. Computational modeling of the forward and reverse problems in instrumented sharp indentation. Acta Mater 2001;49:3899–918.
[27] Shen Y-L, Guo YL. Indentation modelling of heterogeneous materials. Model Simul Mater Sci Eng 2001;9:391–8.
[28] Carlsson S, Larsson P-L. On the determination of residual stress and strain fields by sharp indentation testing. Part II: Experimental investigation. Acta Mater 2001;49:2193–203.
[29] Carlsson S, Larsson P-L. On the determination of residual stress and strain fields by sharp indentation testing. Part I: Theoretical and numerical analysis. Acta Mater 2001;49:2179–91.
[30] Bucaille JL, Felder E. Finite-element analysis of deformation during indentation and scratch tests on elastic-perfectly plastic materials. Philos Mag A 2002;82:2003–12.

[31] Gong X-Y, Pelton AR. ABAQUS analysis on nitinol medical applications. In: ABAQUS. HKS publications; 2002.
[32] Auricchio F, Taylor RL. Shape-memory alloys: modelling and numerical simulations of the finite-strain superelastic behavior. Comput Meth Appl Mech Eng 1997;143:175–94.
[33] Auricchio F, Taylor RL, Lubliner J. Shape-memory alloys: macro-modelling and numerical simulations of the superelastic behavior. Comput Meth Appl Mech Eng 1997;146: 281–312.
[34] Rebelo NG, Gong X-Y, Connally M. Finite element analysis of nitinol's plastic behaviour. In: Proceedings of the international conference on shape memory and superelastic technologies. SPIE; 2003. p. 501–7.
[35] Huang W. Yield surfaces of shape memory alloys and their applications. Acta Mater 1999;47:2769–76.
[36] Gao XY, Huang WM. Transformation start stress in non-textured shape memory alloys. Smart Mater Struct 2002;11: 256–68.
[37] Lexcellent C, Blanc P. Phase transformation yield surface determination for some shape memory alloys. Acta Mater 2004;11: 2317–24.
[38] Otsuka K, Wayman CM. Mechanism of shape memory effect and superelasticity. In: Otsuka K, Wayman CM, editors. Shape Memory Mater. Cambridge: CUP; 1998. p. 27–48.